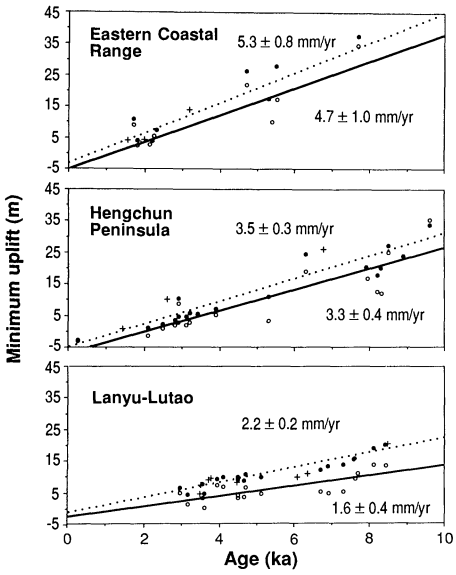


**Fig. 3.** Plots of minimum uplift versus sample age for the three study areas. The enclosed circles and dashed regression lines are for data points with altitudes corrected by the generalized sea level curve (*14*), whereas the open circles and solid regression lines are corrected according to the East China Sea curve (*15*). The slopes of these lines represent average uplift rates. Based on the errors shown (standard error of the regression), there is no significant difference in results with the use of either sea level curve for altitude correction. Crosses represent $^{14}C$ ages with altitudes corrected by the generalized sea level curve. Abbreviations: ka, thousand years ago; yr, year.

lands, northeast of Taiwan (*17*). The moderately high uplift rate indicated for the southern peninsular area may be related to the recently proposed eastward-plunging subduction zone in southern Taiwan, centered at about 22°N (*18*). The uplift rates are in accord with the seismically based interpretation that subduction is important in the southern part of the country, although its effects are perhaps less evident during the Holocene.

Our analysis of the distribution and age of elevated coral samples across an active convergent margin in Taiwan has shown that uplift has persisted at a reasonably uniform rate through the Holocene. Comparison to other collisional boundaries must await similar investigations across other zones of tectonic convergence.


REFERENCES AND NOTES

1. C. S. Ho, *Mem. Geol. Soc. China* 7, 15 (1986).
2. S. B. Yu and C. Lee, *Tectonophysics* **125**, 73 (1986); E. Barrier and J. Angelier, *ibid.*, p. 39; Y. B. Tsai, *Mem. Geol. Soc. China* 7, 353 (1986); J. F. Stephan *et al.*, *ibid.*, p. 231.
3. C. C. Liu, *The 6th Symposium on Science and Technology of Surveying and Mapping*, C. T. Shih, Ed. (Chung-Cheng Institute of Technology, Taoyuan, Taiwan, 1987) (in Chinese); C. C. Liu and S. B. Yu, *Tectonophysics* (special issue), in press.
4. T. H. Peng, Y. H. Li, F. T. Wu, *Mem. Geol. Soc. China* **2**, 57 (1977).
5. Samples were collected only from what appeared to be in situ outcrops. Hand specimens were examined in the field with a hand lens and those with obvious recrystallization effects were rejected. Other field criteria followed are outlined in A. L. Bloom, W. S. Broecker, J. M. A. Chappell, R. K. Matthews, and K. J. Mesolella [*Quat. Res. (N.Y.)* **4**, 185 (1974)].
6. In all, 14 samples were analyzed in Tallahassee [Florida State University (FSU)] and 43 samples were analyzed in Taipei [Institute of Earth Sciences (IES)] including 12 replicates of samples run at FSU. A regression of calculated $^{230}Th$ ages based on uranium-series measurements of these replicates showed that, on average, the IES ages equaled 95% of the FSU ages [$(\Sigma dev^2/\{n-2\})^{1/2} = 960$ years]. Both laboratories used temperature-controlled ion-exchange and rotating-disc electrodeposition procedures [W. J. McCabe, R. G. Ditchburn, N. E. Whitehead, *Inst. Nuclear Sci. (New Zealand) Rep. INS-R-262* (1979), p. 29; R. G. Ditchburn and W. J. McCabe, *ibid. INS-R-325* (1984), p. 10; W. C. Burnett, K. B. Baker, P. Chin, W. J. McCabe, R. G. Ditchburn, *Mar. Geol.* **80**, 215 (1988)].
7. C. H. Wang, W. C. Burnett, E. F. Yu, W. C. Tai, *Inst. Earth Sci., Academia Sinica (Republic of China) Rep. ASIES-ER8802* (1988), p. 31; C. F. Lin, thesis, National Taiwan University (1989).
8. Samples analyzed by both $^{14}C$ and uranium-series techniques yielded $^{14}C$ ages equivalent to 98% of the $^{230}Th$ ages [$(\Sigma dev^2/\{n-2\})^{1/2} = 600$ years].
9. W. S. Broecker, D. L. Thurber, J. Goddard, T. L. Ku, *Science* **159**, 297 (1968); T. L. Ku, *J. Geophy. Res.* **73**, 2271 (1968); H. H. Veeh and W. C. Burnett, in *Uranium-Series Disequilibrium: Applications to Environmental Problems*, M. Ivanovich and R. S. Harmon, Eds. (Clarendon, Oxford, 1982), pp. 459–480.
10. Out of 49 samples analyzed, none had a $^{232}Th$ concentration higher than 0.04 ppm.
11. R. H. Randall and Y. M. Cheng, *Acta Geol. Taiwanica* **19**, 79 (1977); R. H. Randall and Y. M. Cheng, *ibid.* **20**, 1 (1979).
12. J. A. Clarke, W. E. Farrell, W. R. Peltier, *Quat. Res. (N.Y.)* **9**, 265 (1978); J. A. Clarke and C. S. Lingle, *ibid.* **11**, 279 (1979).
13. A useful compilation of sea level curves representing the last 15,000 years may be found in A. L. Bloom, Ed., *IGCP Project 61 Atlas of Sea Level Curves* (Cornell Univ. Press, Ithaca, NY, 1977). See also T. Yoshikawa, Ed., *Inventory of Quaternary Shorelines, Pacific and Indian Oceans Region* (International Union for Quaternary Research, Commission on Quaternary Shorelines, Tokyo University of Agriculture, 1987).
14. F. P. Shepard, *Essays in Marine Geology in Honor of K. O. Emery* (Univ. of Southern California Press, Los Angeles, CA, 1963), p. 1; N. A. Morner, *Quaternaria* **14**, 65 (1971).
15. The East China Sea curve was taken from X. Zhao and J. Zhang as reproduced in Y. Ota [in *Sea Surface Studies: A Global View*, R. J. N. Devoy, Ed. (Croom Helm, London, 1987).
16. Subsequent field inspections revealed that some of our sampling points were significantly influenced by local faulting. We have thus deleted the respective samples (two samples from the Eastern Coastal Region and three samples from the Hengchun Peninsula) in our data analysis and Figs. 2 and 3.
17. K. Konishi, S. O. Schlanger, A. Omura, *Mar. Geol.* **9**, 225 (1970).
18. S. W. Roecker, Y. H. Yeh, Y. B. Tsai, *J. Geophys. Res.* **92**, 10547 (1987).


19. We thank T. K. Liu for his help in the $^{14}C$ dating. T. Tseng, H. L. Zen, and K. C. Chang aided in the sample collection. W. C. Tai, C. F. Lin, K. Landing, K. Harada, and H. Narita performed the uranium-series analyses. Helpful reviews of this manuscript were provided by J. P. Chanton and J. B. Cowart. This study was supported by the National Science Council of the Republic of China (contracts No. 77-0202-M001-10 and 77-0204-M001-02), Academia Sinica Research Fund, and the National Science Foundation (INT-8620107).

30 October 1989; accepted 15 February 1990


# Indication of Increasing Solar Ultraviolet-B Radiation Flux in Alpine Regions


MARIO BLUMTHALER AND WALTER AMBACH



**Measurements at the Jungfraujoch High Mountain Station (Swiss Alps, 47°N, 3576 meters above sea level) indicate that there has been a slight increase of about 1 percent per year in the flux of solar ultraviolet-B radiation (290 to 330 nanometers) since 1981. A Robertson-Berger detector was used to measure solar erythemal radiation. The increase can be related to a long-term ozone depletion.**


WITH DEPLETION OF STRATOspheric ozone ($O_3$), the flux of solar ultraviolet-B radiation (UVB) (290 to 330 nm) reaching the earth's surface should increase. Such an increase could have various consequences; in particular, it could increase the risk of skin cancer (*1–3*). In the Northern Hemisphere, a slight $O_3$ depletion of approximately 3% from 1969 to 1986 has been reported (*4*), in contrast to a considerable $O_3$ depletion over Antarctica in October (*5*). Earlier studies have not detected an increase in the UVB flux corresponding to the $O_3$ depletion in the Northern Hemisphere, however (*6–8*). Detection of a slight long-term increase is not easy, because the flux of UVB reaching the earth is influenced by numerous atmospheric conditions, apart from $O_3$ content. Changes in aerosol concentration, in cloudiness, and in the reflectivity of the earth's surface due to varying snow cover affect the flux of UVB. In addition, there is a strong natural seasonal variation of the $O_3$ content in mid-latitudes (*9*). All these effects lead to a large variability in the flux of UVB at the earth's surface; this variability can mask a tendency toward a slight increase.

In order to minimize the effects of these masking parameters and to identify long-term effects of decreasing $O_3$ concentrations


Institute of Medical Physics, University of Innsbruck, Muellerstrasse 44, A-6020 Innsbruck, Austria.

on UVB, we have taken the following aspects into consideration:

1) In the Northern Hemisphere we have measured UVB and global radiation (solar radiation at wavelengths between 300 and 2000 nm) at a high mountain station (Jungfraujoch, Swiss Alps, 47°N, 3576 m above sea level) from 1981 to 1989. Both radiation fluxes were measured simultaneously at the same site.

2) We analyzed the flux ratio of UVB to global radiation (UVB/G) instead of the UVB flux alone. Using this ratio reduces some of the effects of processes that control both UVB and global radiation.

3) The Alpine high mountain station was used because the aerosol concentration there is small compared with that in urban areas. Moreover, effects of fluctuations of aerosol concentration are minimized by the use of the flux ratio.

4) We restricted the analysis to cloudless days and daily totals; thus, the influence of clouds was eliminated. Clouds filter UVB less than global radiation (*10*), and therefore the influence of clouds is not eliminated by use of the flux ratio.

5) We analyzed residuals, which were calculated as the deviations of the individual values of UVB/G from the values, represented by a smoothed seasonal course. Thus, the influence of the natural seasonal variation of $O_3$ was eliminated and the long-term trend of UVB can be analyzed.

We made measurements during 13 individual periods of approximately 8 weeks each from 1981 to 1989 (*11*). We measured UVB with a Robertson-Berger detector. The spectral sensitivity of this detector was adjusted to the action spectrum of human skin erythema (*12, 13*). Nevertheless, at longer wavelengths the detector is somewhat more sensitive than human skin; hence the response of the detector to an $O_3$ reduction is somewhat less than for human skin. Because the erythema reaction is considered to be representative for numerous biological reactions, catalyzed by UVB (*14*), the detector indicates the biologically effective UVB. The data are given in sunburn units (SU), where 1 SU corresponds to the threshold dose for erythema (*15*). The long-term stability of the Robertson-Berger detector was controlled by permanent comparisons among four detectors at our station one with another, and by repeated comparisons with a standard detector, provided by the manufacturer. This standard detector was checked frequently against a calibrating light source at the Health Sciences Center, Temple University, Philadelphia. The influence of the detector temperature on the result was taken into consideration (*16*). Global radiation was measured with a pyranometer,

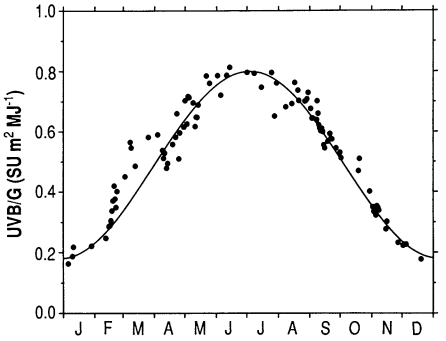


**Fig. 1.** Seasonal variation of UVB/G as derived from daily totals on cloudless days from 1981 to 1989, measured at the high mountain station Jungfraujoch. The solid line represents the best fit to the data.

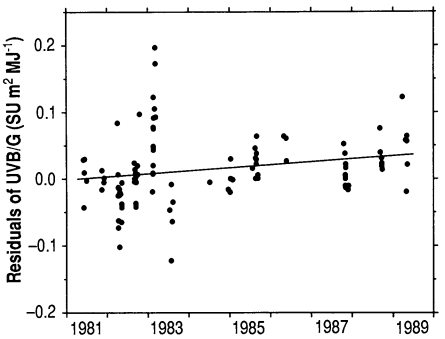


**Fig. 2.** Long-term tendency of the residuals of UVB/G from 1981 to 1989. The solid line represents the regression line.

and daily totals are in megajoules per meter squared. The pyranometer was calibrated regularly in the field by means of an actinometer, and the stability of the actinometer was checked several times at the World Radiation Center in Davos, Switzerland. The detectors were permanently controlled with respect to dirt or precipitation on the quartz domes. Because of these controls, we suggest that the data for both UVB and global radiation are not influenced by systematic errors.

In analyzing the data, we fitted all the individual values for the period 1981 to 1989 with a curve representing the variations in a single seasonal course (Fig. 1). This seasonal course is controlled by both the variation of solar elevation and the variation of $O_3$ content. The value of UVB/G reaches a maximum in summer, because at high solar elevations the optical path length through the $O_3$ layer is small. Only UVB is strongly reduced by absorption in the $O_3$ layer and not global radiation. In addition, the seasonal course is not symmetrical to the summer solstice, because the natural seasonal variation of $O_3$ content in mid-latitudes causes the $O_3$ concentration to be lower in autumn than in spring.

The residuals [see (*5*)] are the differences between the individual values and the best fitting seasonal curve for all the data, which is given by the function $y = 0.49 + 0.31 \sin[0.0168 + (x - 90)]$, where $y$ is UVB/G and $x$ is the number of the day in the course of the year. Use of the residuals thus eliminates the influence of seasonal variations of solar elevation, stratospheric $O_3$ concentration, and cosine response error in the evaluation.

Analysis of the residuals shows that the later data tend to yield positive residuals, whereas the early data show negative residuals from the best-fit seasonal curve (Fig. 2). Scattering of the residuals reflects daily $O_3$ variations. The slope and SD of the regression line are $0.00534 \pm 0.00198$ SU $m^2$ $MJ^{-1}$ $year^{-1}$, significantly different from 0 ($P < 0.01$). The significance of the positive slope of the relation is independent of the fitting function of the seasonal variation in the grouped data. This positive slope suggests that either (i) UVB has increased as compared with global radiation or (ii) global radiation has decreased as compared with UVB. Because there is no indication that global radiation has decreased significantly during recent years, we interpret the positive slope as reflecting an increase in the intensity of UVB since 1981. Compared to the mean value of UVB/G (0.49 SU $m^2$ $MJ^{-1}$, Fig. 1), the data indicate that the increase in UVB was $1.1 \pm 0.4\%$ per year from 1981 to 1989. The percentage increase depends strongly on the reference value selected, however. If the maximum of UVB/G (0.8 SU $m^2$ $MJ^{-1}$, Fig. 1) is used instead, the increase is only $0.7 \pm 0.2\%$ per year.

This trend of a slight increase in UVB is in qualitative agreement with the reported slight $O_3$ depletion in the Northern Hemisphere of about 3% from 1969 to 1986 (*4*). The results of daily column $O_3$ measurements made with a Dobson spectrophotometer in Arosa, Switzerland, also show a slight $O_3$ depletion of 4% from 1969 to 1988 (*17*). The influence of tropospheric $O_3$ is reduced at our high-altitude station as compared with stations at lower altitudes.

The analysis of residuals shows that particularly high values of UVB flux were measured in the spring of 1983. These high values are a reflection of the increased UVB flux related to the reduced $O_3$ content after the eruptions of El Chichon volcano (*18–20*). If the exceptional spring 1983 data are omitted from the analysis of the residuals, the trend of increasing UVB will be augmented.

## REFERENCES AND NOTES

1. F. Urbach, *The Biologic Effects of Ultraviolet Radiation* (Pergamon, New York, 1969).
2. P. Cutchis, *Science* **184**, 13 (1974).

3. I. M. Basset, M. A. Box, R. G. Hewitt, *Search* **5** (no. 5), 182 (1974).
4. R. T. Watson and Ozone Trends Panel, M. J. Prather and Ad Hoc Theory Panel, and M. J. Kurylo and NASA Panel for Data Evaluation, "Present state of knowledge of the upper atmosphere 1988: An assessment report" [*NASA RP-1208*, National Aeronautics and Space Administration (NASA) Office of Space Science and Application, Washington, DC, 1988].
5. M. J. Prather, M. B. McElroy, S. C. Wofsy, *Nature* **312**, 227 (1984); World Meteorological Organization, *Atmospheric Ozone 1985, Assessment of Our Understanding of the Process Controlling Its Present Distribution and Change* (NASA, Washington, DC, 1986); R. T. Watson, M. A. Geller, R. S. Stolarski, R. F. Hampson, *NASA RP-1162* (1986); L. B. Callis and M. Natarajan, *Nature* **323**, 772 (1986); J. C. Farman, B. G. Gardiner, J. D. Shanklin, *ibid.* **315**, 207 (1985); S. Solomon, R. R. Garcia, F. S. Rowland, D. J. Wuebbles, *ibid.* **321**, 755 (1986).
6. J. Scotto, G. Cotton, F. Urbach, D. Berger, T. Fears, *Science* **239**, 762 (1988).
7. D. S. Berger and F. Urbach, *Photochem. Photobiol.* **35**, 187 (1982).
8. D. S. Berger, in *Human Exposure to Ultraviolet Radiation: Risks and Regulations*, W. F. Passchier and B. F. M. Bosnjakovic, Eds. (Elsevier, New York, 1987), pp. 213–221.
9. N. Robinson, *Solar Radiation* (Elsevier, New York, 1966), p. 114.
10. M. Blumthaler and W. Ambach, *Atmos. Environ.* **22**, 749 (1988).
11. ———, H. Canaval, *Photochem. Photobiol.* **42**, 147 (1985).
12. D. S. Berger, *ibid.* **24**, 587 (1976).
13. B. L. Diffey, *ibid.* **46**, 55 (1987).
14. D. H. Sliney, *Am. Ind. Hyg. Assoc. J.* **33**, 644 (1972).
15. J. DeLuisi and J. Harris, *Atmos. Environ.* **17**, 751 (1983).
16. M. Blumthaler and W. Ambach, *Arch. Meteorol. Geophys. Bioklimatol. Ser. B* **36**, 357 (1986).
17. J. Staehelin and H. Dütsch, *Chimia* **43**, 338 (1989).
18. J. Slomka, *Publ. Inst. Geophys. Pol. Acad. Sci. D* **30** (220), 163 (1988).
19. H. T. Mantis, C. S. Zerefos, A. Bais, I. Ziomas, A. Kelessis, *Arch. Meteorol. Geophys. Bioklimatol. Ser. B* **36**, 135 (1986).
20. J. K. Angell, J. Korshover, W. G. Planet, *Mon. Weather Rev.* **113**, 641 (1985).
21. We thank the head of the High Alpine Research Station Jungfraujoch, Bern, for assistance. Supported by the Austrian Academy of Sciences, Vienna.

12 October 1989; accepted 8 February 1990

# Phosphate-Methylated DNA Aimed at HIV-1 RNA Loops and Integrated DNA Inhibits Viral Infectivity

HENK M. BUCK, LEO H. KOOLE, MARCEL H. P. VAN GENDEREN, LIA SMIT, JAN L. M. C. GEELEN, SUZANNE JURRIAANS, JAAP GOUDSMIT

**Phosphate-methylated DNA hybridizes strongly and specifically to natural DNA and RNA. Hybridization to single-stranded and double-stranded DNA leads to site-selective blocking of replication and transcription. Phosphate-methylated DNA was used to interrupt the life cycle of the human immunodeficiency virus type–1 (HIV-1), the causative agent of acquired immunodeficiency syndrome (AIDS). Both antisense and sense phosphate-methylated DNA 20-nucleotide oligomers, targeted at the transactivator responsive region and the primer binding site, caused complete inhibition of viral infectivity at a low concentration. Hybridization of phosphate-methylated DNA with folded and unfolded RNA was studied by ultraviolet and proton nuclear magnetic resonance spectroscopy. The combined results of hybridization studies and biological experiments suggest that the design of effective antisense phosphate-methylated DNA should focus on hairpin loop structures in the viral RNA. For sense systems, the 5′ end of the integrated viral genome is considered to be the important target site.**

IT HAS BEEN SHOWN THAT PHOSPHOrothioate, phosphoramidate, and methyl phosphonate oligodeoxynucleotides are potential antiviral agents because their specific hybridization to viral sequences leads to inhibition of replication and gene expression, and because they are very resistant to cellular exo- and endonucleases (*1–3*). In principle, neutrally charged backbones will lead to strong hybridization (as a consequence of the absence of interstrand phosphate-phosphate charge repulsions), stability toward nucleases, and facile transport through cell membranes (*4*). Phosphate-methylated DNA shows particular promise in that this neutral modification exhibits the best conformational accommodation to natural DNA and RNA (*5–7*) (Fig. 1A).

Our initial experiments on the strength of hybridization of phosphate-methylated DNA with natural single-stranded DNA are shown in Fig. 1B. Hybridization of phosphate-methylated d(GGA.ATC.CTG.CAG) with its natural complement shows a transition temperature ($T_m$) of 55°C, whereas the corresponding natural duplex does not exist in salt-free solution. Addition of 0.1*M* NaCl, which diminishes interstrand phosphate-phosphate charge repulsions since the $Na^+$ ions tend to neutralize the negative phosphate charges, results in a $T_m$ of 42°C for the natural duplex and represents a physiological salt solution. For hybridization with unfolded RNA, we studied the duplex formation of phosphate-methylated d($C_n$) ($n$ = 3, 5, 10, and 20) with poly(rG) (*8*). The $T_m$ values were 13°, 28°, 36°, and 51°C, respectively. For comparison, natural d($C_n$) ($n$ = 3, 5, 10, and 20) did not associate with poly(rG) under the condition of 0.1*M* NaCl. Phosphate-methylated DNA–natural DNA duplexes are more stable than phosphate-methylated DNA-RNA duplexes

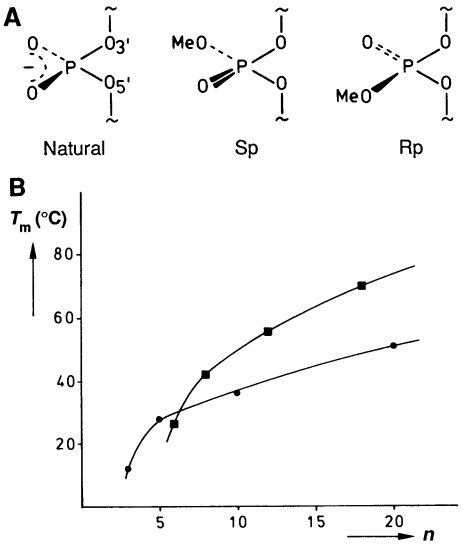


**Fig. 1.** (**A**) Structural formulas of natural phosphate, and $S_p$ and $R_p$ methyl phosphotriester groups. Investigations on the dinucleotide systems d(TpT), d(ApT), d(ApC), d(ApA), d(GpC), d(CpC), and d(TpC) with 600-MHz proton NMR spectroscopy (*5*) revealed that the diastereoisomeric phosphate-methylated forms possess virtually identical conformational features in aqueous solution, which closely resemble a right-handed B helix structure (*27*), namely $C_{2'}$-endo puckered sugar rings: $R_p$ 59%, $S_p$ 60%, and natural 61%; $\gamma^+(C_{4'}\text{-}C_{5'}$ backbone bond): $R_p$ 63%, $S_p$ 57%, and natural 59%; $\beta^t(C_{5'}\text{-}O_{5'}$ bond): $R_p$ 66%, $S_p$ 69%, and natural 84% (percentages denote time-averaged contribution of these conformations). $R_p$, $S_p$, and natural systems show anti orientation of the bases. (**B**) Duplex ⇄ coil $T_m$'s for hybrids of phosphate-methylated DNA oligomers of length $n$, with complementary natural DNA (■) and RNA (●), as determined with ultraviolet (UV) hyperchromicity. The total nucleotide concentration in all experiments was 2 μ*M*. $T_m$ values were independent of the ionic strength of the solution, which was consistent with the absence of interstrand phosphate-phosphate charge repulsions. Melting transitions occurred within 10°C intervals, implying that hybridization was equally strong for all diastereoisomeric forms (*28*). The duplexes of phosphate-methylated d(GGA.ATC), d(AGC.CTG.AC) and d(CAC.TCA.CCC.ATG.AAC.AGC) with their natural complements displayed $T_m$ values of 27°, 42°, and 70°C, respectively (*6*).

H. M. Buck, L. H. Koole, M. H. P. van Genderen, Department of Organic Chemistry, Eindhoven University of Technology, P.O. Box 513, 5600 MB Eindhoven, The Netherlands.
L. Smit, J. L. M. C. Geelen, S. Jurriaans, J. Goudsmit, Human Retrovirus Laboratory, AMC, Department of Virology, Meibergdreef 15, 1105 AZ Amsterdam, The Netherlands.